BERNOULLI-GAUSSIAN SPECTRAL ANALYSIS OF UNEVENLY SPACED ASTROPHYSICAL DATA

Sébastien Bourguignon, Hervé Carfantan

Laboratoire d'Astrophysique de l'Observatoire Midi-Pyrénées, UMR 5572 CNRS/UPS
14 avenue Edouard Belin, 31400 TOULOUSE, France
bourgui@ast.obs-mip.fr, Herve.Carfantan@obs-mip.fr

ABSTRACT

We address the problem of line spectra detection and estimation from astrophysical data. As observations generally suffer sampling irregularities, false peaks may appear in the Fourier spectrum. We propose a linear spectral model with an arbitrarily large number of fixed frequencies and search for a sparse solution by modelling the spectrum as a Bernoulli-Gaussian process. The use of Markov Chain Monte Carlo methods to compute the posterior mean estimate is discussed in the unsupervised framework. The original work by Cheng *et al.* [1] is modified to account for specificities of the spectral analysis problem. Simulations reveal the efficiency of the method and its relevance to the astrophysical frequency detection context is emphasized. Finally, an application to astrophysical data is presented.

1. INTRODUCTION

Many astrophysical phenomena involve periodic behaviours, as the orbital motions in multiple systems or the oscillations of variable stars. The basis for their study is the search for periodicities in their observed light curves - *i.e.* the evolution of their radiation over time - that correspond to spectral lines in the frequency domain. Astronomical time series generally suffer uneven sampling with periodic gaps. Then, undesirable lobes appear in the Fourier spectrum, which is therefore inappropriate for the estimation of line spectra. Moreover, the number of observations is generally small, so that *high resolution* methods have to be considered. As an example, a signal issued from Herbig Ae star HD 104237 observations during 5 observing nights is plotted on figure 1 with its Fourier spectrum.

Spectral analysis has recently been addressed as an inverse problem and solutions have been proposed through the Bayesian framework. The direct identification of a multisinusoidal model [2] is attractive, but its adaptation to irregularly sampled data has still to be studied. Furthermore, the multisinusoidal model is very strong and may be unadapted in the frequent case where the data spectrum include very low frequency components, such as data shown on figure 1. The formulation as a linear model with a large number of fixed frequencies leads to the simplified problem of searching for a *sparse* vector of spectral amplitudes. The regularization framework [3] allows to perform sparse solutions, that can be adapted to the irregular sampling case [4].This approach, however, is limited when aiming at an unsupervised procedure and does not provide any confidence level complementary to the estimation.

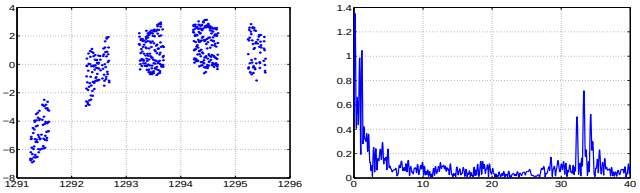

Fig. 1. HD 104237 data (left) and Fourier spectrum (right).

The interest of the stronger Bernoulli-Gaussian (BG) spectral model for line spectra estimation has been addressed [5] with maximum *a posteriori* (MAP) estimation. In a blind seismic deconvolution context, Cheng *et al.* [1] perform the Posterior Mean (PM) estimation of both the convolution wavelet and the BG data sequence using a Gibbs sampler. We propose to apply a similar strategy to the spectral analysis problem with slightly different objectives. In our case, we focus on the unsupervised and high resolution estimation of the frequencies and amplitudes of the spectral lines and the associated *confidence level*, which is crucial information in astronomy. A modification is introduced to the Gibbs sampler proposed in [1], which increases its efficiency for the frequency detection problem. The MCMC based PM estimation and its complementary variance analysis are shown to give satisfactory simulation results. Finally, an application to astrophysical data is presented where stellar oscillations are detected from low-frequency perturbated raw data.

2. MODEL AND ESTIMATION FRAMEWORK

2.1. Bernoulli-Gaussian model

Let $\boldsymbol{y} = \{y(t_n)\}_{n=1\dots N}$ be the observed data at sampling times t_n. Data are modelled as a noisy sum of an arbitrarily large number P of sinusoids with discretized frequencies on the grid $\mathcal{G} = \{f_k\}_{k=0\dots P} \triangleq \{\frac{k}{P} f_{\max}\}_{k=0\dots P}$:

$$y(t_n) = \sum_{k=0}^{P} a_k \cos 2\pi f_k t_n + b_k \sin 2\pi f_k t_n + \epsilon_n$$

It is convenient to introduce $\boldsymbol{x}_k = (a_k, b_k)$ and the $2(P+1)$ vector $\boldsymbol{x} = (\boldsymbol{x}_0, \dots, \boldsymbol{x}_P)^T$, so that model writes:

$$\boldsymbol{y} = \mathbf{W}\boldsymbol{x} + \boldsymbol{\epsilon} \tag{1}$$

where $\mathbf{W}_{n,2k} = \cos(2\pi f_k t_n)$, $\mathbf{W}_{n,2k+1} = \sin(2\pi f_k t_n)$ and the white sequence $\boldsymbol{\epsilon}$ stands for the perturbations (model errors, measurement errors and additive noise). In the following, ϵ_n are supposed independent and identically distributed (*i.i.d.*) with normal distribution $\epsilon_n \sim \mathcal{N}(0, \sigma_\epsilon^2)$. Note that astronomical data are generally irregularly sampled, which makes the alias-free frequency range wider than in the regular sampling case [6]. Then, no Nyquist maximum frequency is defined and parameter $f_{\max}$ has to be set according to some physical prior information.

As only a small number of non zero spectral parameters $\boldsymbol{x}_k$ are searched, sequence $\boldsymbol{x}$ is modelled as a Bernoulli-Gaussian (BG) process. The frequencies of the signal are supposed *i.i.d.* on the grid $\mathcal{G}$ with the same probability of appearance λ, and conditionally to the presence of a line, the corresponding amplitudes follow a normal distribution. A low value of parameter λ then controls the number of spectral lines. Let $\boldsymbol{q} = (q_0 \dots q_P)$ be a sequence of Bernoulli random variables that control the presence of spectral lines along the grid $\mathcal{G}$: $Pr(q_k = 1) = \lambda$, $Pr(q_k = 0) = 1 - \lambda$. Variables $a_k|q_k$ and $b_k|q_k$ are supposed $\overset{i.i.d.}{\sim} \mathcal{N}(0, q_k\sigma^2)$ [1] or equivalently $p(\boldsymbol{x}_k|q_k) = g_2(\boldsymbol{x}_k, q_k\sigma^2\mathbf{I}_2)$ where $g_m(\boldsymbol{u}, \boldsymbol{\Sigma})$ stands for the m-variate centered gaussian distribution:

$$g_m(\boldsymbol{u}, \boldsymbol{\Sigma}) = \frac{1}{(2\pi)^{N/2}|\boldsymbol{\Sigma}|^{1/2}} e^{-\frac{1}{2}\boldsymbol{u}^T\boldsymbol{\Sigma}^{-1}\boldsymbol{u}}$$

As q_k is implicitly defined by the value of $\boldsymbol{x}_k$, hereafter $\boldsymbol{x}$ stands for $(\boldsymbol{q}, \boldsymbol{x})$ when there is no ambiguity. Note that the particular case $k = 0$ corresponds to a slightly different prior with $b_0 = 0$ and $a_0|q_0 \sim \mathcal{N}(0, 2\sigma^2)$. For the sake of clarity, the consequent modifications are not specified in the following calculations.

With hyperparameters $\boldsymbol{\theta} = (\lambda, \sigma^2, \sigma_\epsilon^2)$, the posterior distribution writes by Bayes rule:

$$\begin{aligned} p(\boldsymbol{x}|\boldsymbol{y}, \boldsymbol{\theta}) &\propto p(\boldsymbol{y}|\boldsymbol{x}, \boldsymbol{\theta}) p(\boldsymbol{x}|\boldsymbol{\theta}) \\ &\propto g_N(\boldsymbol{y} - \mathbf{W}\boldsymbol{x}, \sigma_\epsilon^2\mathbf{I}_N) \\ &\quad \times \prod_{k=0}^{P} \lambda g_2(\boldsymbol{x}_k, \sigma_x^2\mathbf{I}_2) + (1-\lambda) g_2(\boldsymbol{x}_k, \mathbf{0}) \end{aligned} \tag{2}$$

2.2. Hyperparameters

The Bayesian framework allows to consider unsupervised estimation by jointly estimating $(\boldsymbol{x}, \boldsymbol{\theta})$ from $p(\boldsymbol{x}, \boldsymbol{\theta}|\boldsymbol{y}) \propto p(\boldsymbol{x}|\boldsymbol{y}, \boldsymbol{\theta}) p(\boldsymbol{\theta})$ with prior information $p(\boldsymbol{\theta})$ on the hyperparameters. We consider here uniform priors for $(\lambda, \sigma_\epsilon^2)$ on $[0, 1] \times [0, +\infty[$ and a vague inverse-gamma *conjugate* prior [1] is adopted on $\sigma^2 \sim \mathcal{IG}(\alpha, \beta)$, centered on the power of the observed signal and with a large variance. In the following we set α and β such that $\mathbf{E}[\sigma^2] = \boldsymbol{y}^T\boldsymbol{y}/N$ and $\mathbf{E}[(\sigma^2)^2] = 100$. Procedure is then unsupervised and these prior choices guarantee the integrability of $p(\boldsymbol{x}|\boldsymbol{y}, \boldsymbol{\theta}) p(\boldsymbol{\theta})$ *w.r.t.* $\boldsymbol{\theta}$, which is a necessary condition for sampling from the joint ditribution $p(\boldsymbol{x}, \boldsymbol{\theta}|\boldsymbol{y})$ with MCMC methods [7].

2.3. Estimation strategy

The BG deconvolution problem has largely been addressed within the maximum a posteriori (MAP) estimation framework. Original work by Kormylo *et al.* [8] propose to maximize the posterior likelihood $Pr(\boldsymbol{q}|\boldsymbol{y})$ w.r.t. $\boldsymbol{q}$ first, and then posteriorly estimate the corresponding amplitudes. The resulting combinatorial optimization problem, however, requires the use of *suboptimal* optimization methods such as the *Single Most Likely Replacement* (SMLR) iterative algorithm. Moreover, this approach becomes computationally expensive when aiming at an unsupervised procedure [9].

We propose to compute the posterior mean (PM) estimate of the spectral parameters $\boldsymbol{x}$:

$$\widehat{\boldsymbol{x}}_{\text{PM}} = \mathbb{E}[\boldsymbol{x}|\boldsymbol{y}, \boldsymbol{\theta}] = \int \boldsymbol{x}\, p(\boldsymbol{x}|\boldsymbol{y}, \boldsymbol{\theta})\, d\boldsymbol{x}$$

using Markov Chain Monte Carlo methods (MCMC). The motivations for performing the PM estimate in our case are manifold. First, the computation of $\widehat{\boldsymbol{x}}_{\text{PM}}$ by MCMC makes it possible to derive a confidence level associated to every period detection, which is an essential point: this approach allows to compute both a probability of appearance for each spectral line (through the estimation of the Bernoulli sequence $\boldsymbol{q}$) and also a variance associated to the corresponding spectral amplitude. Then, it can be shown that sampling from the target distribution $p(\boldsymbol{x}|\boldsymbol{y}, \theta)$ is computationally more attractive than sampling from $Pr(\boldsymbol{q}|\boldsymbol{y}, \theta)$. Last, the unsupervised estimation objective is possible by jointly sampling from $p(\boldsymbol{x}, \boldsymbol{\theta}|\boldsymbol{y})$ at the same computational cost.

[1] For $q_k = 0$, $\mathcal{N}(0, q_k\sigma^2)$ (resp. $g_m(\boldsymbol{x}_k, q_k\sigma^2\mathbf{I}_2)$) may be viewed as the limiting case $\mathcal{N}(0, \sigma_k^2), \sigma_k^2 \to 0$ (resp. $g_m(\boldsymbol{x}_k, \sigma_k^2\mathbf{I}_2), \sigma_k^2 \to 0$).

3. A MODIFIED GIBBS SAMPLING ALGORITHM

A Gibbs sampling algorithm is particularly suited to the generation of $(\boldsymbol{x}^{(t)}, \boldsymbol{\theta}^{(t)}) \sim p(\boldsymbol{x}, \boldsymbol{\theta}|\boldsymbol{y})$, as the conditional distributions $p(\boldsymbol{x}_k|\boldsymbol{x}_{-k}, \boldsymbol{\theta}, \boldsymbol{y})$ – where $\boldsymbol{x}_{-k} \triangleq \{\boldsymbol{x}_\ell\}_{\ell \neq k}$ – have a BG expression and $p(\theta_i|\boldsymbol{\theta}_{-i}, \boldsymbol{x}, \boldsymbol{y})$ belong to usual families of probability density functions.

As the spectral model (1) uses bidimensional parameters $\boldsymbol{x}_k = (a_k, b_k)$, the expressions derived in [1] are slightly modified. Introducing the $N \times 2$ matrix $\boldsymbol{w}_k = [\cos 2\pi f_k t_n, \sin 2\pi f_k t_n]_{n=1\ldots N}$ and $\boldsymbol{e}_k = \boldsymbol{y} - \sum_{l \neq k} \boldsymbol{w}_l \boldsymbol{x}_l^T$, the conditional posterior distribution of $\boldsymbol{x}_k$ writes:

$$p(\boldsymbol{x}_k|\boldsymbol{x}_{-k}, \boldsymbol{y}, \boldsymbol{\theta}) = \lambda_k \, g_2(\boldsymbol{x}_k - \boldsymbol{\mu}_k, \mathbf{R}_k) + (1 - \lambda_k) \, g_2(\boldsymbol{x}_k, \mathbf{0}) \quad (3)$$

with: $\lambda_k = \frac{\widetilde{\lambda}_k}{\widetilde{\lambda}_k + (1-\lambda)}$, $\widetilde{\lambda}_k = \frac{\lambda}{\sigma^2} |\mathbf{R}_k|^{1/2} e^{\boldsymbol{\mu}_k^T \mathbf{R}_k^{-1} \boldsymbol{\mu}_k}$,

$$\mathbf{R}_k^{-1} = \frac{\mathbf{I}_2}{\sigma^2} + \frac{1}{\sigma_\epsilon^2} \boldsymbol{w}_k^T \boldsymbol{w}_k, \; \boldsymbol{\mu}_k = \frac{1}{\sigma_\epsilon^2} \mathbf{R}_k \boldsymbol{w}_k^T \boldsymbol{e}_k$$

Since $\boldsymbol{x}_0 = (a_0, 0)$, the case $k = 0$ leads to slightly different expressions which are straightforward to derive.

The corresponding conditional posterior distributions on the hyperparameters write:

$$\begin{aligned}
\lambda|\boldsymbol{x}, \boldsymbol{y}, \sigma, \sigma_\epsilon &\sim \mathcal{B}e(M + 1, P + 1 - M) \\
\sigma^2|\boldsymbol{x}, \boldsymbol{y}, \lambda, \sigma_\epsilon &\sim \begin{cases} \mathcal{IG}(M + \alpha, ||\boldsymbol{x}||^2/2 + \beta) \text{ if } \boldsymbol{x}_0 = \mathbf{0} \\ \mathcal{IG}(M + \alpha - 1/2, ||\boldsymbol{x}||^2/2 + \beta) \text{ else} \end{cases} \\
\sigma_\epsilon^2|\boldsymbol{x}, \boldsymbol{y}, \lambda, \sigma &\sim \mathcal{IG}(N/2 - 1, ||\boldsymbol{y} - \mathbf{W}\boldsymbol{x}||^2/2)
\end{aligned}$$

where M is the number of non zero components in $\boldsymbol{x}$, and $\mathcal{B}e$ stand for the beta distribution.

Drawing samples iteratively from above conditional posterior distributions leads to the classical Gibbs sampler. However, convergence of Gibbs sampling methods is known to be slowed down by the attraction of the chain towards local modes of the target distribution [7, p. 205]. Practical experience in the spectral analysis problem shows a critical behaviour when a sample $\boldsymbol{x}^{(t)}$ models a true line (with index k_0) with two lines on each side (with indexes $k_0 - 1$ and $k_0 + 1$) and a zero value for the true frequency location (see figure 2, configuration A). As the Gibbs sampler only performs one move at a time, removing a line or adding a third one in the middle leads to a model with a much lower probability: parameter λ_{k_0} in equation (3) takes very low values while $\lambda_{k_0-1}, \lambda_{k_0+1} \simeq 1$. Thus, the chain hardly escapes from a configuration such as A.

This pathological behaviour of the Gibbs sampler is to be compared to the limitations of the SMLR suboptimal optimization strategy. As each iteration only changes one value of the Bernoulli sequence $\boldsymbol{q}$, several steps are needed to move from configuration A to configuration B, and intermediate steps may lead to a lower posterior probability.

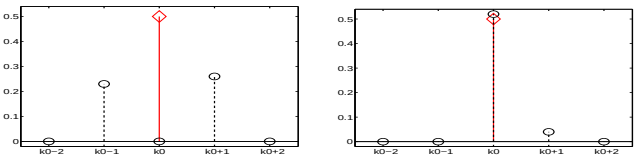

Confi guration A Confi guration B

Fig. 2. Left: true line ($\diamond$) and critical sample $\boldsymbol{X}^{(t)}$ ($\circ$). Right: $\boldsymbol{X}^{(t+1)}$ after a successful resampling step. Here $X_k \triangleq \sqrt{a_k^2 + b_k^2}$ stands for the spectral amplitude at frequency f_k.

Consequently, such a detector gets stuck in a local maximum corresponding to configuration A. These problems are pointed out by Chi and Mendel [10] who propose additional transitions moving a current line one point left or right. In an analogous way, we include a new sampling step to the usual Gibbs sampler, that enables one point frequency shifts. For a current sample $\boldsymbol{x}^{(t)}$ with Bernoulli sequence $\boldsymbol{q}^{(t)}$, the following step is proposed:

a) select k_0 randomly among $\{k; q_k^{(t)} \neq 0\}$

b) with probability 0.5, set $\delta k = 1$, else set $\delta k = -1$, and propose the new Bernoulli sequence $\boldsymbol{q}'$ with:
$$\begin{cases} q'_\ell = 1 - q_\ell^{(t)}, & \text{if } l = k_0 \text{ or } l = k_0 + \delta k \\ q'_\ell = q_\ell^{(t)} & \text{else} \end{cases}$$

c) compute the corresponding amplitudes $\boldsymbol{x}'$ as the minimum variance estimator of $(\boldsymbol{x}|\boldsymbol{q}', \boldsymbol{y}, \boldsymbol{\theta})$ [8]

d) accept the move if the posterior distribution (2) is increased: $(\boldsymbol{q}^{(t+1)}, \boldsymbol{x}^{(t+1)}) = (\boldsymbol{q}', \boldsymbol{x}')$ if $\rho > 1$ (else $(\boldsymbol{q}^{(t+1)}, \boldsymbol{x}^{(t+1)}) = (\boldsymbol{q}^{(t)}, \boldsymbol{x}^{(t)})$) with:

$$\begin{aligned}
\rho &= \frac{p(\boldsymbol{q}', \boldsymbol{x}'|\boldsymbol{y}, \boldsymbol{\theta})}{p(\boldsymbol{q}^{(t)}, \boldsymbol{x}^{(t)}|\boldsymbol{y}, \boldsymbol{\theta})} \\
&= \exp -\frac{1}{2\sigma_b^2}(||\boldsymbol{y} - \mathbf{W}\boldsymbol{x}'||^2 - ||\boldsymbol{y} - \mathbf{W}\boldsymbol{x}^{(t)}||^2) \\
&\quad \times \exp -\frac{1}{2\sigma^2} \left(\sum_k ||\boldsymbol{x}'_k||^2 - \sum_k ||\boldsymbol{x}_k^{(t)}||^2 \right)
\end{aligned}$$

In practice, this additional step allows to jump from configuration A to a configuration B with two adjacent lines (b). Then, the corresponding amplitude estimation (c) will associate a high value to the spectral amplitude at the true frequency, as shown on figure 2, model B, where the left line has been shifted right. Note that this resampling step is not a Metropolis-Hastings step, but can better be interpreted as a burn-in procedure. In practice, this step is proposed with a probability $\mu^{(t)}$ decreasing exponentially to 0 when $t \to +\infty$, which ensures the asymptotic convergence of the chain to the interest posterior distribution (2).

4. SIMULATION RESULTS

Signal shown on figure 3 is the sum of 5 sinusoids with frequencies $f_{i,i=1\ldots5}$ from 0.1 to 0.16 Hz, corrupted by 10 dB white gaussian noise. The $N = 250$ data are irregularly sampled with additional periodic gaps. This kind of spectrum simulates the rotational splitting effect on variable stars. Sampling gaps cause high lobes in the spectral window, and the Fourier spectrum of the data is unsatisfactory in terms of peak detection, as shown on figure 3.

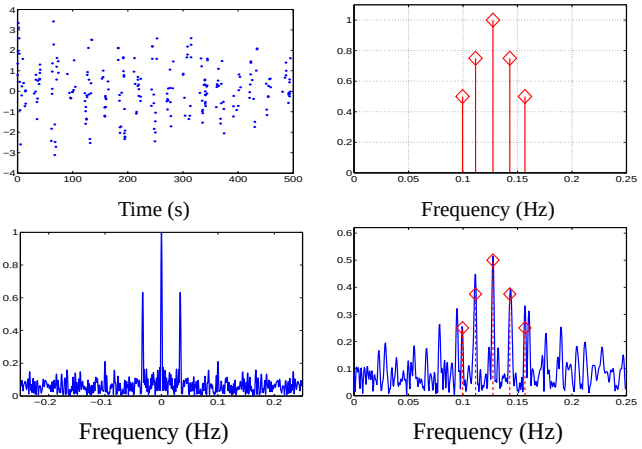

Fig. 3. Top: test signal (left) and true spectral lines (right). Bottom: spectral window (left) and Fourier spectrum (right).

Samples $\boldsymbol{x}^{(t)}, \boldsymbol{\theta}^{(t)} \sim p(\boldsymbol{x}, \boldsymbol{\theta}|\boldsymbol{y})$ are drawn using algorithm of section 3 for $P = 500$ frequencies. After T iterations, PM estimates $\widehat{\boldsymbol{x}}_T$ and $\widehat{\boldsymbol{\theta}}_T$ are computed: $(\widehat{\boldsymbol{x}}_T, \widehat{\boldsymbol{\theta}}_T) = \frac{2}{T}\sum_{T/2+1}^{T}(\boldsymbol{x}^{(t)}, \boldsymbol{\theta}^{(t)})$. Associated variances $\widehat{\sigma}^2_{\boldsymbol{x}}$ and $\widehat{\sigma}^2_{\boldsymbol{\theta}}$ are also computed as the variances of the chain $(\boldsymbol{x}^{(t)}, \boldsymbol{\theta}^{(t)})$. As there is no general convergence test [7], we propose to stop algorithm when $||\widehat{\boldsymbol{x}}_T - \widehat{\boldsymbol{x}}_{T-1}||_\infty < \nu$, $||\widehat{\boldsymbol{\theta}}_T - \widehat{\boldsymbol{\theta}}_{T-1}|| < \nu$, with $\nu = 10^{-3}$. This heuristic criterion has shown satisfactory practical results for this problem. Results are shown on figure 4. The underlying PM estimate of the Bernoulli sequence $\widehat{\boldsymbol{q}}$ shows posterior probabilities equal to 1 at the closest approximations of the true frequencies on grid $\mathcal{G}$ and with very low values elsewhere, and the corresponding spectrum shows an accurate amplitude estimation with a low associated variance. Note that in this simulation with well-resolved frequencies, the supervised SMLR algorithm also provides satisfactory results. In our case, however, additional information on the estimator variance is obtained and the procedure is fully unsupervised. Finally, figure 5 briefly illustrates a typical situation where maximization algorithms as SMLR fail. Two close frequencies separated by three grid steps are considered with 10 dB SNR and $N = 100$ irregularly sampled data. Due to the close frequency mix, the SMLR algorithm is unable to correctly localize the two lines. Note that the SMLR algorithm was implemented with the « correct » hyperparameters values (λ is the average number of lines, σ^2 is the mean of the squared amplitudes and σ_b^2 the noise variance), while the proposed PM estimation is fully unsupervised.

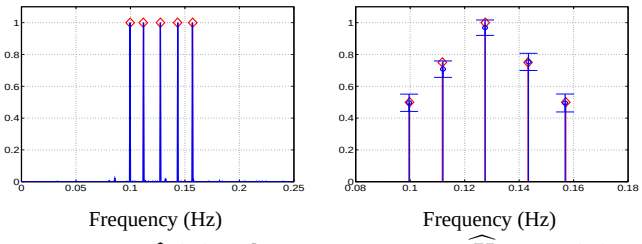

Estimate $\widehat{\boldsymbol{q}}$ $(-)$ and true frequency locations $(\diamond)$

Estimate $\widehat{\boldsymbol{X}} \pm \sigma_{\widehat{\boldsymbol{X}}}$ $(-)$ and true spectrum $(\diamond)$

Fig. 4. BG estimation results

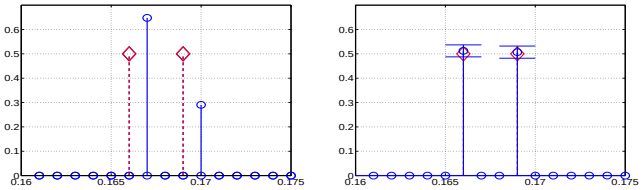

Fig. 5. Simulation results with 2 close spectral lines $(\diamond)$. Left: SMLR solution. Right: $\widehat{\boldsymbol{X}} \pm \sigma_{\widehat{\boldsymbol{X}}}$.

5. APPLICATION TO ASTROPHYSICAL DATA

We propose to perform the spectral estimation of the signal presented on figure 1, which is the radial velocity curve of Herbig Ae star HD 104237 for 5 observing nights. This is a multiple object system and the main orbital motion generates a low frequency behaviour on the global velocity curve. Moreover, the primary star of the system is supposed to be pulsating, so that several oscillation modes are expected. Due to the day/night alternation, the spectral window shows a high secondary lobe at frequency 1 day^{-1} and the Fourier spectrum only emphasizes one peak around 33 day^{-1} and 1 day^{-1} aliases. Note that the `clean` deconvolution method, widely used in astrophysics, also fails because of the low frequency perturbations. Note that the `clean` deconvolution method, widely used in astrophysics (see *e.g.* [11]), also fails because of the low frequency perturbations. Estimation results are shown on figure 6, where several spectral lines are detected around 33 day $^{-1}$ in addition to the main low frequency energy. Five lines are detected with a high probability (superior to 98%). Other non-zero spectral amplitudes appear that have a lower probabil-

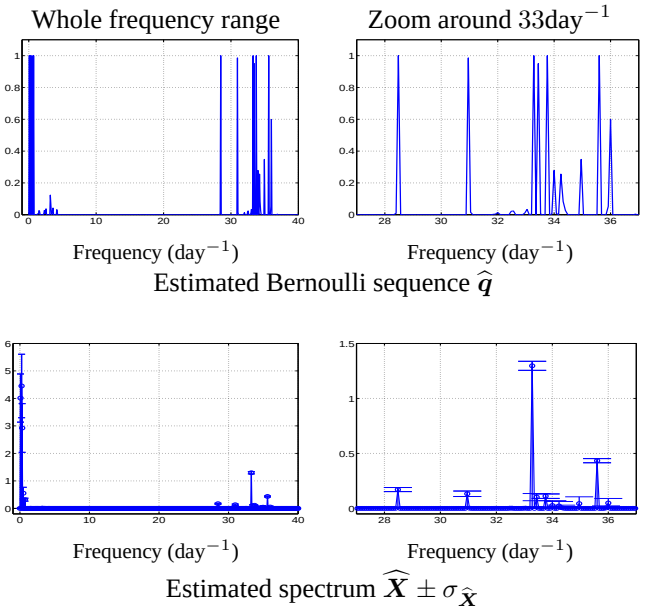

Fig. 6. Estimation results on HD 104237 data.

ity, and the large associated variances are due to the average effect between zero and non-zero values along the chain. To make this spectral estimator more readable, we suggest to first estimate the frequencies as those having a posterior probability of appearance superior to a given threshold and then compute the amplitude means and variances conditionnally to the presence of a corresponding line along the chain, *i.e.* by averaging only the spectral samples $\boldsymbol{x}_k^{(t)}$ corresponding to $q_k^{(t)} = 1$. Results of this reestimation are shown on figure 7 where only the lines corresponding to a posterior probability $\widehat{q}_k > 98\%$ are conserved. As the detected frequencies are typical values of δ Scuti pulsations, this is a satisfactory result for the validation of this method on experimental data. We must note, however, that such a result is not systematically obtained depending on the initialization of the random generator. Actually, it has been found that the slow convergence of the Gibbs sampler makes it hard to know whether the convergence to the interest distribution has been obtained or if the chain has got stuck in some local mode of the distribution. The modification introduced in section 3 aims at solving this problem, but the frequency of this move, which has to decrease towards 0 when the number of iterations $T \rightarrow +\infty$, has shown to be a critical parameter to tune on this experimental data.

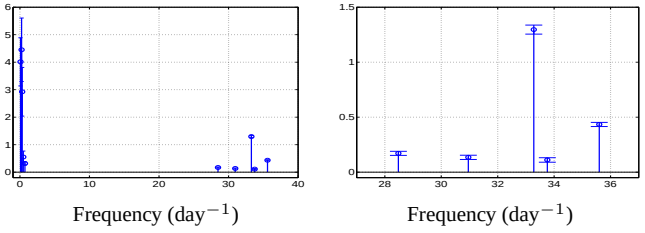

Fig. 7. Estimation results on HD 104237 data: amplitude conditional reestimation. Left: whole frequency range, right: zoom around 33 day^{-1}

6. CONCLUSION

This paper presented an application of the MCMC-based estimation of Bernoulli Gaussian processes introduced by Cheng *et al.* [1], adapted to the estimation of line spectra from unevenly sampled data. The proposed method allows to compute the posterior mean estimates of the spectral parameters and their associated variances in an unsupervised manner. A modification to the usual Gibbs sampler was introduced to accelerate the convergence by means of an efficient burn-in procedure. Satisfactory simulation results were obtained and application to astrophysical data revealed the ability of the method to retrieve spectral lines in the presence of low frequency perturbations. However, application to experimental data also illustrated some difficulties inherent to the use of MCMC methods, as the use of an appropriate convergence criterion and the necessity of a post-processing step.

A future work should include the proposed modification of the Gibbs sampler in a Hastings-Metropolis step and then build a properly hybrid algorithm, avoiding the tuning inherent to the burn-in process.

7. REFERENCES

[1] Q. Cheng, R. Chen, and T.-H. Li, Simultaneous wavelet estimation and deconvolution of reflection seismic signals," *IEEE Trans. on Geoscience and Remote Sensing*, vol. 34, no. 2, pp. 377–384, Mar. 1996.

[2] C. Andrieu and A. Doucet, Joint bayesian model selection and estimation of noisy sinusoids via reversible jump MCMC," *IEEE Trans. on Signal Processing*, vol. 47, no. 10, pp. 2667–2676, Oct. 1999.

[3] M.D. Sacchi, T.J. Ulrych, and C.J. Walker, Interpolation and extrapolation using a high-resolution discrete Fourier transform," *IEEE Trans. on Signal Processing*, vol. 46, no. 1, pp. 31–38, Jan. 1998.

[4] S. Bourguignon, H. Carfantan, and L. Jahan, Regularized spectral analysis of unevenly spaced data," in *Proceedings of ICASSP'05*, Philadelphia, USA, Mar. 2005, vol. 4, pp. 421–424.

[5] F. Dublanchet, *Contribution de la méthodologie bayésienne à l'analyse spectrale de raies pures et à la goniométrie haute résolution*, Thèse de Doctorat, Université de Paris-Sud, Oct. 1996.

[6] L. Eyer and P. Bartholdi, Variable stars: which Nyquist frequency?," *Astronomy and Astrophysics Supplement Series*, vol. 135, pp. 1–3, Feb. 1999.

[7] C. P. Robert, *Méthodes de Monte-Carlo par Chaînes de Markov*, Economica, Paris, 1996.

[8] J. Kormylo and J.M. Mendel, Maximum-likelihood detection and estimation of Bernoulli-Gaussian processes," *IEEE Trans. on Information Theory*, vol. 28, pp. 482–488, 1982.

[9] F. Champagnat, Y. Goussard, and J. Idier, Unsupervised deconvolution of sparse spike trains using stochastic approximation," *IEEE Trans. on Signal Processing*, vol. 44, no. 12, pp. 2988–2998, Dec. 1996.

[10] C.-Y. Chi and J. M. Mendel, Improved maximum-likelihood detection and estimation of Bernoulli-Gaussian processes," *IEEE Trans. on Information Theory*, vol. 30, pp. 429–434, Mar. 1984.

[11] D. H. Roberts, J. Lehar, and J. W. Dreher, Time series analysis with CLEAN. I. Derivation of a spectrum," *The Astronomical Journal*, vol. 93, no. 4, pp. 968–989, Apr. 1987.